Draft version March 3, 2014
Preprint typeset using LaTeX style emulateapj v. 12/16/11

MEASURING GALAXY CLUSTERING WITH FAR-IR LINE INTENSITY MAPPING

B. D. Uzgil[1,2], J. E. Aguirre[1], and C. M. Bradford[2]

Draft version March 3, 2014

ABSTRACT

a new technique to measure galaxy clustering without individual detections of galaxies. We develop robust predictions of line specific intensity for a suite of astrophysically interesting lines and make predictions about the detectability of the clustering signal via the 3D power spectrum of a data cube, where the galaxies need not be either spatially or spectrally resolved. We show that line intensity mapping is an efficient method for imaging spectrometers like SPICA/SAFARI to obtain galaxy clustering measurements down to $k < 0.1\ h\mathrm{Mpc}^{-1}$ and out as far as $z \sim 3$.

Subject headings: far-infrared spectroscopy; galaxy redshift surveys

1. INTRODUCTION

Intensity mapping is a *statistical* analysis of the spatial fluctuations in spectral line emission, whereby a survey of spectral lines at different frequencies produces a fully three dimensional data cube containing "tomographic scans" of the Universe along the spectral (i.e., redshift) direction and is decomposed into its power spectrum. Atomic (Gong et al 2012, Visbal et al 2011, etc.) and molecular (Lidz et al 2011, Gong et al 2012 etc.) transitions – such as the 21 cm spin flip transition from H^{o}, CO (2-1), and [CII] 158μm – have been investigated as candidates for intensity mapping experiments during the Epoch of Reionization. Of these, the neutral hydrogen case is undoubtedly the most developed in terms of its standing in the literature (cf. Furlanetto, Oh, and Briggs for a review) and in the experimental arena (e.g., PAPER (Parsons et al 2010), MWA), and so interest in measuring the [CII] power spectrum, for instance, primarily erupted as a means to complement the 21 cm studies at high redshift via the cross-correlation.

As a proof of principal, the appeal of intensity mapping experiments in the post-Reionization era is obvious. Neutral hydrogen is, again, the most mature in this respect, as 21cm experiments have successfully measured the 21cm-galaxy cross power spectrum (Chang et al 201) or put limits on the 21cm auto-power (Switzer et al 2013), but the detectability of another transition Hydrogen transition, the Lyα line, has also been explored in Pullen et al for redshifts from before Reionization down to $z \sim 2$.

Here we examine the application of the intensity mapping technique to moderate redshifts, targeting the fine structure line emission from ionized carbon in the interstellar medium of star-forming galaxies during $0.5 < z < 1.5$. The [CII]158μm line is a well-suited probe of the galaxy population during this time frame, as the mean dust attenuation in galaxies peaks at $z \sim 1.5$, when roughly 80% of the cosmic star formation rate density is obscured and captured only in the infrared emission of re-processed starlight by dust grains (Burgarella et al 2013). Moreover, this line is typically the brightest FIR emitted from the ISM of galaxies, with luminosities up 0.1% of the IR luminosity.

Due to the spatio-spectral nature of intensity mapping, this technique as applied to [CII] line intensity fluctuations can be a highly complementary probe to recent studies of the 2-dimensional clustering properties of dusty, star-forming galaxies (DSFGs) (see Casey et al 2014 for a review). These studies, using a modification of the "$P(D)$" approach, for example by (**??**), have already shed light on some aspects of the clustering of the most extreme star-forming system from $z = 1-3$, but they are limited by the lack of redshift information, and by the need to include "nuisance parameters" in their estimation of the halo model. From the far-IR to the millimeter, it remains for the future for ALMA or NOEMA to produce redshift surveys with $\sim 10^3$ galaxies, or even further down the road for CCAT. Thus we present a novel method of characterizing the 3D clustering of DSFGs with [CII] intensity mapping, which, importantly, does not rely on detecting individual galaxies in order to measure the power spectrum with high significance.

The organization of this paper is as follows. We have calculated the mean intensity for a suite of fine structure IR emission lines, including the [CII] line, based on the IR luminosity function and empirical line-to-IR luminosity correlations, and present these results in the context of a power spectrum model in Section 2. In Section, 3, we envision a suitable platform—namely a balloon-borne experiment operating at frequencies between 240μm to 420μm—for conducting the [CII] intensity mapping experiment and discuss the feasibility of measuring the [CII] power spectra in terms of the signal-to-noise ratio (SNR). To better assess the value of intensity mapping studies in the case of [CII] at moderate redshifts, and of intensity mapping experiments in general, we compare in Section 4 the performance of measuring the power spectrum with the intensity mapping approach against traditional galaxy surveys that rely on individual detections of sources.

2. SETTING UP PREDICTIONS FOR FAR-IR LINE POWER SPECTRA DURING $0.5 < Z < 3$

Conventional methods for measuring the spatial autocorrelation of galaxies through galaxy surveys rely on the knowledge of the redshift distribution of sources in the survey. Furthermore, they estimate the true three dimensional clustering of galaxies via the angular pro-

badeu@sas.upenn.edu
[1] University of Pennsylvania, Philadelphia, PA 19104
[2] Jet Propulsion Laboratory

jection. Intensity mapping, however, contains intrinsic redshift information and provides a direct measure of the clustering power spectrum in three-dimensional k-space, which makes it a highly complementary probe of structure in the cosmic web.

The complete auto power spectrum of a given FIR line as a function of wavenumber k, $P_{i,i}(k,z)$, can be separated into power from the clustering of galaxies, $P_{i,i}^{clust}(k,z)$ and a Poisson term describing their discrete nature, $P_{i,i}^{shot}(z)$. We compute the full nonlinear matter power spectrum, $P_{nl}(k,z)$, using the publicly available code HALOFIT+, which has been the standard tool for predicting matter power spectra upon its success in fitting state-of-the-art dark matter simulations over a decade ago (Smith et al 2003) . (We note in passing, however, that since that time, authors (cf., e.g., Takahashi et al 2012) have pointed out improvements to the halo model fit on the small scales previously inaccessible due to constraints on simulation resolution.) The clustering component of the line power spectrum is then written as

$$P_{i,i}^{clust}(k,z) = \bar{S}_i^2(z)\bar{b}_i^{2}(z)P_{nl}(k,z). \quad (1)$$

Here we have implicitly assumed that the fluctuations in line emission trace the matter power spectrum with some average bias, $\bar{b}_i(z)$. The mean line intensity, $\bar{S}_i(z)$, in units of Jy sr^{-1}, can be calculated as

$$\bar{S}_i(z) = \int \mathrm{d}n_i \frac{L_i}{4\pi D_L^2} y_i D_A^2, \quad (2)$$

where the integration is taken with respect to n_i, the number of galactic line emitters per cosmological comoving volume element. (The factor y_i is the derivative of the comoving radial distance with respect to the observed frequency, i.e. $y = d\chi/d\nu = \lambda_{i,rest}(1+z)^2/H(z)$, and D_A is the comoving angular distance.)

Finally, the shot noise component of the total line power spectrum—with the same units as the clustering term, namely, Jy^2 sr^{-2} (Mpc h^{-1})^3—takes the form

$$P_{i,i}^{shot}(z) = \int \mathrm{d}n_i \left(\frac{L_i}{4\pi D_L^2}\right)^2 \left(y_i D_A^2\right)^2. \quad (3)$$

2.1. *Calculating IR line volume emissivity*

The number density of line emitters and the line luminosity that appear in equations (2) and (3) can be derived by a variety of methods. In earlier papers on intensity mapping of molecular and fine-structure emission lines at high redshift (z $\gtrsim$ 6), one approach involved using the dark matter halo mass function in lieu of the line emitter density (and invoking a one-to-one correlation between halos and galaxies, which is not unreasonable at high redshifts). The line luminosity, in turn, could be scaled according to the star formation rate, which was related to halo mass via a proportionality constant comprised of factors that described the fraction of baryons available for star formation, as well as the dynamical timescale for star formation and a duty cycle for emission. While this theoretical model is feasible at high redshift to provide an estimate on the mean intensity $\bar{S}_i$, we take advantage of the relative wealth of observations of [CII] luminosities in individual galaxies, IR galaxy number counts, and cosmic star formation rate density at the lower redshifts relevant to this study. To this end, we first employ the empirically-constrained, backwards-evolution model of the IR luminosity function $\Phi(L_{IR},z)$ from Bethermin et al (2011, hereafter B11) to predict the number of galaxies with luminosity L_{IR} at a given redshift in some comoving volume of the Universe per logarithmic luminosity interval, i.e., $\frac{\mathrm{d}N(L_{IR},z)}{\mathrm{d}V\mathrm{dlog}_{10}L_{IR}}$ or $\frac{\mathrm{d}n_{IR}}{\mathrm{dlog}_{10}L_{IR}}$. One major drawback of our empirical approach is that it does not allow us to model the bias in a self-contained manner, e.g., such as in the halo model formalism that other predictions, which connect L_{IR} to halo mass, employ.

To convert the infrared luminosity to a line luminosity, we apply the relation for L_i as a function of L_{IR} provided by Spinoglio et al (2012). The fit in their paper was based on the collection of ISO-LWS observations of local galaxies in Brauher et al (2008), and is reproduced below for [CII]:

$$L_{\mathrm{[CII]158}}(L_{\mathrm{IR}}) = (0.89{\pm}0.03)\mathrm{log}_{10}L_{\mathrm{IR}} - (2.44{\pm}0.07) \quad (4)$$

Thus, it becomes possible to write the cosmic mean intensity and shot noise of the line, in units of Jy sr^{-1}, as a function of redshift based on the B11 luminosity function and Spinoglio et al (2012) $L_i - L_{\mathrm{IR}}$ relation as

$$\bar{S}_{\mathrm{i}}(z) = \int_{L_{IR,min}}^{L_{IR,max}} \mathrm{dlog}L_{IR}\Phi(L_{IR},z)\frac{f_i L_{IR}}{4\pi D_L^2} y D_A^2 \quad (5)$$

$$P_{i,i}^{shot}(z) = \int_{L_{IR,min}}^{L_{IR,max}} \mathrm{dlog}L_{IR}\Phi(L_{IR},z)\left(\frac{f_i L_{IR}}{4\pi D_L^2} y D_A^2\right)^2 \quad (6)$$

where f_i, i.e. $\frac{L_i(L_{IR})}{L_{IR}}$, is the fraction of IR luminosity emitted in line i, as computed from equation (3). In other words, we have written $\bar{S}_i$ and $P_{i,i}^{shot}(z)$ as the first and the second moments of the luminosity function.

It should be noted that the mean line luminosity $\bar{L}_i$ does, in reality, include a contribution from diffuse gas in the intergalactic medium (IGM), yet Gong et al (2012) estimated that the specific intensity of one of the brightest lines typically observed in galaxies, namely [CII], coming from the IGM ranges from $\sim 10^{-3}$ Jy sr^{-1} to ~ 1 Jy sr^{-1} for different physical conditions in the ISM at $z = 1$—a negligible amount compared to the emission from the interstellar medium (ISM) of galaxies.

The resulting mean intensities for a variety of FIR lines are plotted in Figure 1 as functions of redshift and observed frequency. $\bar{S}_\nu$ vs λ_{obs} can be interpreted as identifying the dominant source of fluctuations, according to our model, for a given frequency. As a specific example, if the target line of an observation is [OI]63μm at $z = 1$, it is necessary to distinguish between the target line and interlopers from different redshifts which nonetheless contribute power at the observed frequency. Visbal and Loeb (2010) showed how the cross spectra can be used to differentiate between a target line and a contaminating line (or "bad line", in their words), since emitters at different redshifts will be spatially uncorrelated. For the observed wavelengths of [CII], however, it is apparent from Figure 2 that, with the exception of contributions from [OIII]88μm near $z \sim 0.01$, the [CII] line is not vulnerable to confusion with interlopers.

3. THE [CII] POWER SPECTRUM UP TO $Z = 1.5$

We present in this section predictions for the power spectrum with error bar estimates for a feasible experimental platform, namely, a balloon-borne experiment with uninterrupted spectral coverage in the wavelength range 240 to 420 μm. Fiducial experimental parameters for the telescope mirror, survey area, and total observing time are taken as 2.5 m, 1 deg^2, and 200 hours, respectively, though we explore the effect of varying the parameters on SNR (cf. Table 1).

Predictions for the fiducial case—as computed from the method of combining the cosmological matter power spectrum and the IR LF model outlined in Section 2.1—for the [CII] power spectrum at four redshifts $z = 0.63, 0.88, 1.16$, and 1.48 are shown in Figure 3. (Note that we use $\Delta^2_{[CII]} = k^3 P_{[CII],[CII]}(k)/(2\pi^2)$ when plotting the power spectrum, where the integral of $\Delta^2_{[CII]}$ over logarithmic k bins is equal to the variance in real space.) At these redshifts, respectively, the average linear bias has been assumed to be $\bar{b} = 2.0, 2.3, 2.6$, and 2.9, in line with theoretical predictions from (Cooray and Sheth ???). [*ASIDE*: seems high compared to Fig 6 in Pullen et al 2013.] The crossing of the one-halo and two-halo terms in the power spectrum can be detected with signal to noise at all redshifts. In calculating the power spectrum sensitivity, the two lowest line-of-sight modes are not included, since these will likely be compromised by the necessity of continuum foreground subtraction. The exact effect of continuum subtraction will need to be modeled via simulation.

Error bar estimates and the total SNR for the power spectrum are calculated by assuming a spectrally flat noise power spectrum, so that the noise power in each pixel, P_N, is written as

$$P_N = \sigma_N^2 \frac{V_{pix}}{t_{pix}}, \tag{7}$$

where σ_N^2 is the instrument sensitivity (noise equivalent intensity, or NEI, in units of Jy sr^{-1} s$^{1/2}$, V_{pix} is the volume of a pixel, and t^{pix}_{obs} is the time spent observing on a single pixel. The variance of a measured k, $\sigma^2(k)$, is then written as

$$\sigma^2(k) = \frac{\left(P_{[CII],[CII]}(k) + P_N(k)\right)^2}{N_{modes}}, \tag{8}$$

where N_{modes} is the number of wavemodes that are sampled for a given k bin of some finite width Δlog(k). (We have chosen Δlog(k) = 0.3 for this analysis.)

The total SNR, in turn, is calculated from the expression

$$SNR_{tot} = \sqrt{\sum_{bins} \left(\frac{P_{[CII],[CII]}(k)}{\sigma(k)} \right)^2} \tag{9}$$

In figure XX, we have separated the total SNR into the contributions from clustering and shot noise for the 0.1, 1.0, and 10.0 deg^2 surveys at $z = 0.88$. For all survey geometries, the longest physical dimension is along the line-of-sight, so SNR on the clustering power $P^{clust}_{[CII],[CII]}$ remains ~ 1 for $k < 0.1$ h/Mpc.

Note that it is possible to rewrite P_N in terms of the parameters from Table 1, giving

$$\begin{aligned} P_N &= \left(\sigma_N^2 A_{pix} \Delta r^{pix}_{los}\right) / \left(\frac{t_{survey}}{n_{beams}/N^{spatial}_{instr}} \right) \\ &= \left(\sigma_N^2 A_{pix} \Delta r^{pix}_{los}\right) / \left(\frac{t_{survey} N^{spatial}_{instr}}{A_{survey}/A_{pix}} \right) \\ &= \sigma_N^2 \frac{\Delta r^{pix}_{los} A_{survey}}{t_{survey} N^{spatial}_{instr}} \end{aligned} \tag{10}$$

In this form, it becomes apparent that—with fixed number of spatial pixels, spectral resolution, and total observing time—the only factor driving up the amplitude of noise power is the survey area; the effect of increasing aperture only allows access to higher wavenumbers, which can be useful for subtracting the shot noise from the total power in later steps of data analysis.This behavior is shown clearly in Figure 5, where the SNR is plotted as a function of k for different survey geometries and both mirror diameters. Also seen in Figure 5, the greater number of wavemodes sampled (entering as $N^{-1/2}_{modes}$ in the expression for σ) with the larger survey area does not necessarily compensate for the the increase in P_N. For example, the factor of ten increase in P_N going from $A_{survey} = 1$ to 10 deg^2 is only overcome by the additional modes in the larger survey area for $k < 1$, leading to a higher S/N for these modes. At $k > 1$, the S/N in each mode for the 1 and 10 deg^2 fields becomes comparable.

4. OBSERVATIONAL STRATEGY

Now let us turn to a question regarding the motivation for intensity mapping in general, as well as in the specific case of [CII] at the redshifts relevant to this study. Having identified the galaxy redshift surveys as an alternative method to measure the 3D clustering power spectrum, it is natural to ask: In which regime does intensity mapping measure the power spectrum with higher SNR than the traditional galaxy surveys?

The expressions for SNR on a k bin of interest for galaxy and intensity mapping surveys (denoted, respectively, by the subscripts “GS” and “IM”) are

$$\mathrm{SNR}_{GS} = \frac{\sqrt{N_{modes}}}{1 + 1/(P_{gal}\bar{n}_{gal})} \tag{11}$$

$$\mathrm{SNR}_{IM} = \frac{\sqrt{N_{modes}}}{1 + P_N/\left(\bar{S}_i^2 P_{gal}\right)} \tag{12}$$

To facilitate our comparisons in what follows, we employ toy models for the IR LF (Figure 4) written in the Schechter formalism—parametrized by the usual α, L_*, and ϕ_*—and normalize the total luminosity density to the empirical model from Section 2 (cf. Appendix for details). We stress that these Schechter models are not

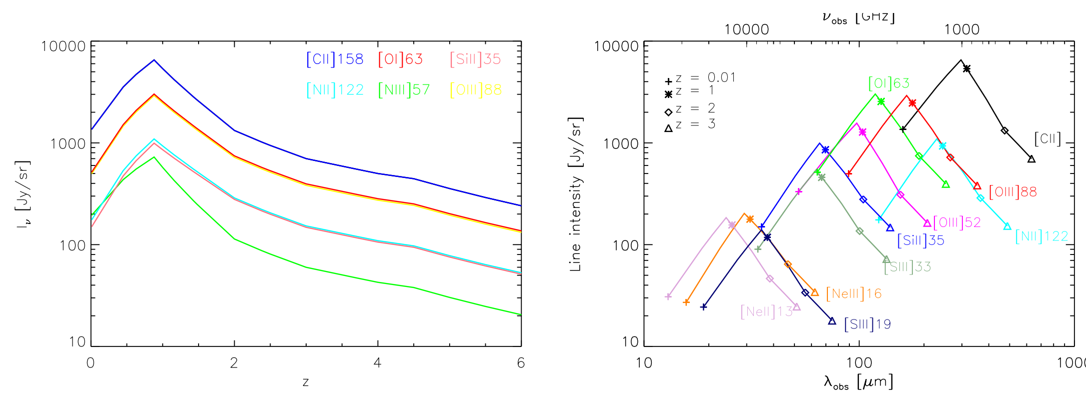

FIG. 1.—: Intensity of fine structure line emission plotted versus redshift (*top*) and observed wavelength (*bottom*) as predicted from Spinoglio line luminosity fits as applied to the Bethermin (2011) luminosity function.

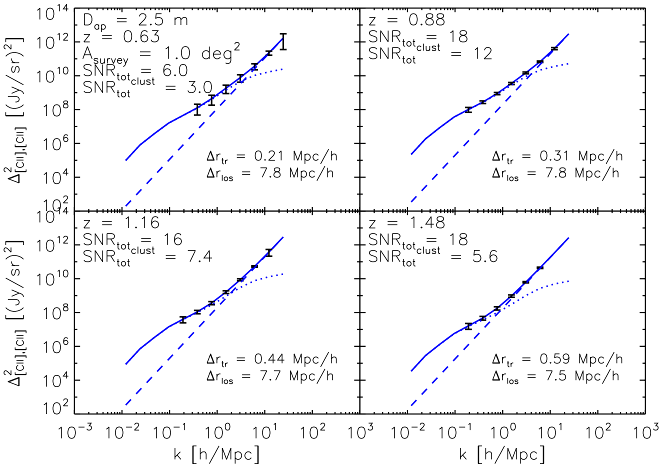

FIG. 2.—: Predicted [CII] power spectra with error bar estimates from $z = 0.63$ to $z = 1.48$ for telescope with 2.5 meter aperture and a survey area of 1 square degree.

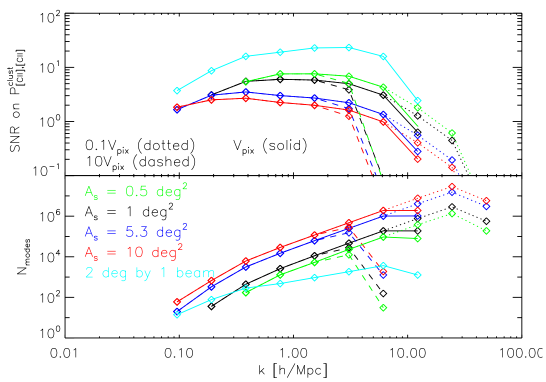

FIG. 3.—: Signal to noise on the clustering term of the [CII] power spectrum $P_{[CII],\,[CII]}$ and number of modes as a function of k. The black, blue, and red lines correspond to survey areas of 1.0, 5.3, and 10.0 deg^2, respectively. Telescopes with apertures yielding 0.1, 1, and 10 times the fiducial pixel volume, V_{pix}, are shown as the dotted, solid, and dashed lines, respectively.

intended to represent a real interpretation of the distribution of galaxies, but are merely helpful for illustrating the effect of the LF *shape* on the relative usefulness of intensity mapping and traditional galaxy surveys.

The line sensitivity, S_γ (units of W m^2 s$^{1/2}$), is the figure of merit for detecting an unresolved line in a point source, and we define individual detections at the 5σ level as having a flux above the instrumental noise in a pixel, i.e., above $5 \times S_\gamma t_{pix}^{-1/2}$. A convenient expression, which explicitly ties the minimum detectable luminosity to a broader framework of experimental variables, for the detection threshold can be written as

$$L_{i,min} = 5 \times f_{err} \rho_i V_{pix}, \tag{13}$$

Here, f_{err} is the fractional error,

$$f_{err} = \left(\frac{\sigma_N}{\sqrt{t_{pix}}}\right) / \bar{S}_i(z) \tag{14}$$

and $\rho_i(z)$ is the comoving luminosity density of line i at

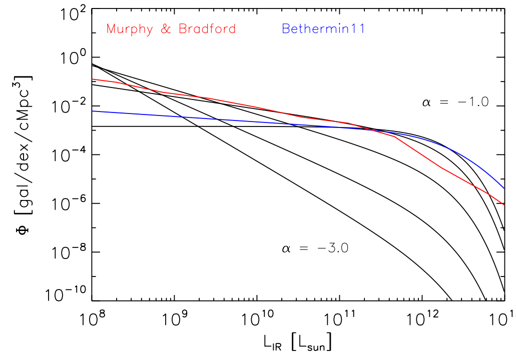

FIG. 4.—: Toy model IR luminosity functions with faint-end slope (from top to bottom) $\alpha = -1.0, -1.5, -2.0, -2.5, -3.0$. The B11 and Muprhy & Bradford models are plotted as blue and red curves, respectively, for comparison.

some z, or $L_* \phi_* \Gamma(2+\alpha, L/L_*)$ in the Schechter notation, so that

$$\frac{L_{i,min}}{4\pi D_L^2} \Leftrightarrow 5 \times S_\gamma t_{pix}^{-1/2} \tag{15}$$

Recall that the units of $\frac{\sigma_N}{\sqrt{t_{pix}}}$ and S_i are Jy sr^{-1}, which does not depend on aperture. For this analysis, we assume the galaxy surveys have reliable spectroscopic redshifts and thus neglect the problem of confusion noise when estimating $L_{i,min}$.

Written in this way, the expression for the detection threshold $L_{i,min}$ already provides some insight as to the optimal regimes for intensity mapping and galaxy surveys. Firstly, for $L_{i,min} \ll L_*$, we expect the galaxy surveys to be an effective means of studying the galaxy population, since the number of detections will be high and the shot noise term will be low. Conversely, if $L_{i,min} \gg L_*$, then the galaxy survey will not be able to detect a significant fraction of galaxies that comprise the faint-end of the luminosity function, and intensity mapping becomes the ideal survey method, since it is sensitive to the total emission at a given redshift.

Now, suppose the voxels are changed in size by some factor ϵ due to a change in aperture diameter by $\sqrt{\epsilon}$, but the survey area and survey observing time are left the same, leading to the following transformations on t_{pix}, the large scale clustering modes N_{modes}^{clust}, P_N, f_{err}, and, ultimately, $L_{i,min}$

$$t_{pix} \rightarrow t'_{pix} \quad = \epsilon t_{pix} \tag{16}$$

$$N_{modes}^{clust} \rightarrow N_{modes}^{clust\prime} \ = N_{modes}^{clust} \tag{17}$$

$$P_N \rightarrow P'_N \quad = P_N \tag{18}$$

$$f_{err} \rightarrow f'_{err} \quad = \frac{f_{err}}{\sqrt{\epsilon}} \tag{19}$$

$$L_{i,min} \rightarrow L'_{i,min} = \sqrt{\epsilon} L_{i,min} \tag{20}$$

We take a moment to point out that an increase in aperture diameter by $\sqrt{\epsilon}$ also results in an increase in the righthand side of Equation 15 by the same factor $\sqrt{\epsilon}$ that appears in Equation 20 after applying the analogous transformations for the line sensitivity:

TABLE 1: Experimental Parameters for Envisioned Balloon Experiment

t_{obs}^{survey} (hr)	200																	
z	0.88									1.48								
$\bar{S}_{[CII]}$ (Jy sr^{-1})	6.57×10^3									2.59×10^3								
NEI (Jy sr^{-1} sec$^{1/2}$)	2.1×10^7									1.0×10^7								
Wavelength Range (μm)	276-317									365-420								
δ_ν (GHz)	2.25									1.70								
A_s (deg^2)	1.0			5.3			10.0			1.0			5.3			10.0		
V_s (Mpc^3 h^{-3})	6.90×10^5			3.66×10^6			6.89×10^6			1.40×10^6			7.42×10^6			1.40×10^7		
P_N (10^{11}Jy^2 sr^{-2} Mpc^3 h^{-3})	2.64			140			264			1.22			6.44			121		
D_{ap} (m)	0.8	2.5	8.0	0.8	2.5	8.0	0.8	2.5	8.0	0.8	2.5	8.0	0.8	2.5	8.0	0.8	2.5	8.0
Beam FWHM (arcmin)	0.16	0.50	1.6	0.16	0.50	1.6	0.16	0.50	1.6	0.16	0.50	1.6	0.16	0.50	1.6	0.16	0.50	1.6
t_{pix} (hr)	0.0345	0.345	3.45	0.00651	0.0651	0.651	0.00345	0.0345	0.345	0.0604	0.604	6.04	0.0114	0.114	1.14	0.00604	0.0604	0.604
SNR_{tot}	35	20	15	16	10	8.4	12	7.8	6.5	48	19	10.1	21	8.5	4.9	16	6.3	3.8
SNR_{tot}^{clust}	14	14	15	7.8	7.8	7.6	6.1	6.1	6.1	7.1	7.3	6.9	3.7	3.7	3.6	2.8	2.9	2.9

$$S_\gamma \rightarrow S'_\gamma = \epsilon S_\gamma \tag{21}$$

$$t_{pix} \rightarrow t'_{pix} = \epsilon t_{pix} \tag{22}$$

$$\tag{23}$$

Thus, the increase of $L_{i,min}$ with V_{pix} suggests that traditional galaxy surveys with large voxels, such that $L_* \phi_* \Gamma(2+\alpha, L/L_*) V_{pix} \gg 1$, will find themselves in the disabling condition of having many sources that are below the detection threshold in a single voxel. On the other hand, because the intensity mapping method does not aim to detect individual galaxies, it will still be able to measure clustering in the large voxel limit with high SNR. We juxtapose in Figure 5 the SNR for the fiducial intensity mapping experiment and galaxy surveys in both the large and small pixel limit in the context of our example for the [CII] power spectrum at $z = 1.5$. As seen in the previous section, a change in aperture does not affect the SNR_{IM} for $k < 0.1$ h/Mpc, but, as expected, dramatically enhances or degrades the capability of galaxy surveys in measuring the power spectrum. From Figure 5 it is clear that the fiducial intensity mapping experiment outperforms galaxy surveys at $z = 1.5$ for all varieties of the tested luminosity functions, and, that this disparity is enhanced in the large pixel limit. In the small pixel limit however, where we expect the galaxy surveys to be capable of measuring the power spectrum with high significance, we see that it becomes important to consider the shape of the luminosity function when drawing conclusions about whether to intensity map or perform a traditional galaxy survey. In fact, it seems that only for the flattest luminosity functions does the small pixel limit improve $\mathrm{SNR}_{tot,GS}$ such that it becomes higher than $\mathrm{SNR}_{tot,GS}$.

In Figure **??**, the SNR for the galaxy surveys is broken down in terms of the number of 5σ detections (top panel) and the observed luminosity density, $\rho_{[CII]}$, relative to the total [CII] luminosity density, $\rho_{[CII]}$ (bottom panel). In the small pixel limit, the galaxy survey reaches SNR ~ 10 at $t_{obs}^{survey} = 700$ hours, at which time it detects $\sim 1,000$ galaxies. In sum, these galaxies account for roughly half of $\rho_{[CII]}$ at $z = 1.5$. Recall that $\frac{\rho_{[CII],obs}}{\rho_{[CII]}} = 1$ for intensity mapping at all observing times.

Another scenario in which an experiment finds itself in the large pixel limit is for observations at long wavelengths. Figure **??** shows the envisioned balloon-borne experiment performing a 5.3 deg^2 survey map of [CII] between $z = 5.4$ and $z = 6.6$, with central frequency now redshifted to 270 GHz (corresponding to $z = 6.0$) and spectral resolution $R = 450$. At these frequencies, we use an estimated NEI that is achievable by instruments for use with the future telescope CCAT, namely, 1.1×10^6 Jy sr^{-1} s$^{1/2}$, which corresponds to line sensitivities for our fiducial aperture of 2.5m and the CCAT 25.0 m aperture of 1.8×10^{-18} and 1.5×10^{-20} W m^{-2} s$^{1/2}$, respectively. As expected, in the long wavelength limit, the relative performance of the [CII] intensity mapping survey and the traditional galaxy surveys in measuring the galaxy clustering becomes more disparate than at $z = 1.5$, in favor of intensity mapping. Again, in the left panel of Figure , which compares intensity mapping and galaxy surveys in the flattest of the three Schechter models considered here, the small pixel limit (here, where V_{pix} is 0.01 times the fiducial value and represents to a CCAT pixel) provides a regime where the galaxy surveys could potentially measure $P_{[CII],[CII]}$ with higher SNR than intensity mapping in a smaller amount of time than it would take intensity mapping experiments to reach the same SNR. But if we look at the fraction of [CII] luminosity density captured by the observed sample (Figure **??**) is $\sim 20\%$ and rises above $\sim 50\%$ after 3,000 hours of observing time. The intensity mapping experiment in the case of the flattest Schechter function model reaches comparable SNR in 8,000 hours. Thus, it does not seem beneficial to intensity map if the luminosity function is indeed very flat at high redshift. For steeper LFs, however, the intensity mapping experiment becomes the ideal observing technique.

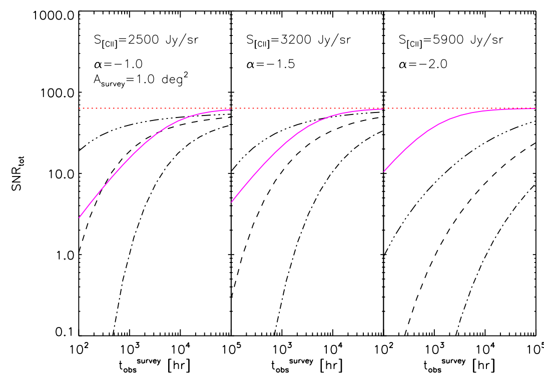

Fig. 5.—: Total Signal-to-Noise ratio (SNR_{tot}) on the clustering power spectrum of [CII] at $z = 1.5$ as a function of the survey observing time (in hours). SNR_{tot} as computed from intensity mapping—which depends only on the integral of the luminosity function, and not the shape—and from the Schechter function models are plotted. Magenta curves represent the intensity mapping experiment. Cyan, black, and green dashed lines correspond to galaxy survey experiments with pixel volumes 0.1, 1.0, 10.0 times the fiducial value. The horizontal dotted *red line* is the maximum SNR, set by the number of modes in the survey volume. Note that the mean [CII] intensity is increasing for decreasing faint-end slopes, which is a consequence of fixing the total IR light for a given Schechter model to the B11 value, and then applying the $L_{[CII]} - L_{IR}$ relation to predict [CII] luminosity.

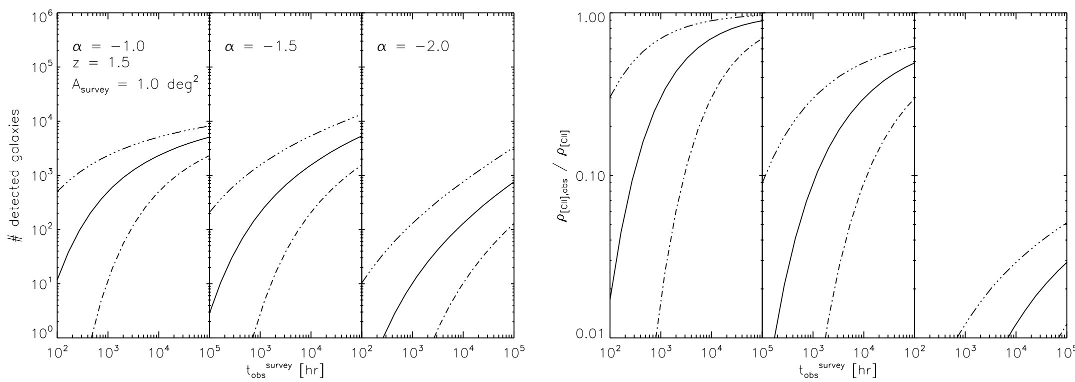

FIG. 6.—: The predicted number of [CII]-detected galaxies and observed fraction of [CII] intensity as a function of observing time for the square degree field. Solid, dash-triple-dotted, and dash-dotted curves represent the fiducial V_{pix}, $0.1V_{pix}$, and $10V_{pix}$, resp.